Chapter 2

Single molecule spectroscopy: fundamentals and beyond

Overview

In section 2.1, the photophysics of fluorescent molecules and the current state of knowledge in selected areas of single molecule spectroscopy (SMS) relevant to the scope of this thesis will be covered. After giving a short overview of the history of single molecule detection (SMD) in solution in section 2.2 and discussing the scanning confocal optical microscopy (SCOM) and its scientific relevance in section 2.3, I will concentrate on several applications, namely the single pair fluorescence resonance energy transfer (spFRET) in section 2.4, the fluorescence correlation spectroscopy (FCS) in section 2.5, and the 3D-orientation determination of single molecules in section 2.6. Section 2.7 will deal with methods, which have been suggested to geometrically confine molecules yielding smaller detection volumes.

2.1 The photophysics of single molecules

This section deals with the photophysics of single molecule experiments and follows the lines of references [77, 99, 112].
The photophysics of fluorescent molecules is usually illustrated using a Jablonski diagram. Figure 2.1 shows a simplified version of a three level system neglecting possible vibronic states. By absorbing a photon from a laser source with a rate constant of k_{exc} the molecule is excited from the ground state S_0 to the first excited singlet state S_1. The rate constant k_{exc} is defined as $k_{exc} = \sigma I/\hbar\omega$, where σ represents the absorption cross section of the molecule, I the applied laser intensity and $\hbar\omega$ the photon energy. A molecule in the S_1 state can undergo different relaxation processes:

- the singlet state S_1 can relax to S_0 by emitting a photon at a radiative rate constant k_{10}
- S_1 can relax to S_0 by *internal conversion* with a non-radiative rate constant k_{ic}
- the molecule can *bleach* with a rate constant k_{bl}

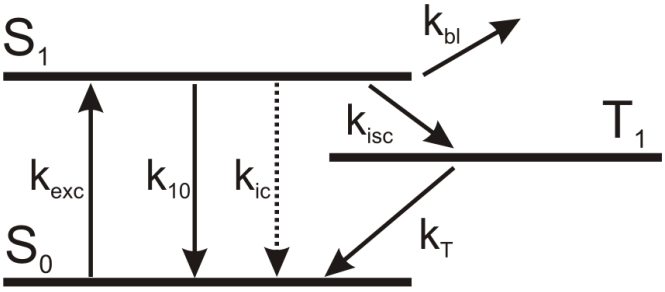

Figure 2.1: Simplified Jablonski diagram showing the transition pathways for a fluorescent molecule. The three level system consists of a ground state S_0, an excited singlet state S_1 and a triplet state T_1. The rate constants k_i are explained in the text.

- S_1 can undergo a spin-forbidden *intersystem crossing* to the first triplet state T_1 with non-radiative rate constant k_{isc}

An occupied triplet state T_1 can relax to S_0 with the rate constant k_T. In most cases, this process is non-radiative for single fluorescent molecules. Taking these relations into account, one can formulate a system of differential equations, which describes the occupancy of the different states as a function of time. If the probability of occupancy for the i-th state is given by ρ_i then the rate equation system reads

$$\begin{aligned} \frac{d}{dt}\rho_{S_0} &= -k_{exc}\rho_{S_0} + k_{10}\rho_{S_1} + k_{ic}\rho_{S_1} + k_T\rho_{T_1} \\ \frac{d}{dt}\rho_{S_1} &= k_{exc}\rho_{S_0} - k_{10}\rho_{S_1} - k_{ic}\rho_{S_1} - k_{isc}\rho_{S_1} - k_{bl}\rho_{S_1} \\ \frac{d}{dt}\rho_{T_1} &= k_{isc}\rho_{S_1} - k_T\rho_{T_1}. \end{aligned} \tag{2.1}$$

The term $k_{bl}\rho_{S_1}$ is often neglected for the calculations, but still remains a limiting factor for single molecule experiments. Still, the solution of the rate equation system is quite complicated. A less complex approach is the stationary case, where the derivatives are set to $\frac{d}{dt}\rho_{S_0} = \frac{d}{dt}\rho_{S_1} = \frac{d}{dt}\rho_{T_1} = 0$ and the normalization condition is $1 = \rho_{S_0} + \rho_{S_1} + \rho_{T_1}$. If the photon emission rate is defined as $R = k_{10}\rho_{S_1}$, then R reads

$$R = \frac{k_{10}}{1 + \frac{k_{isc}}{k_T} + \frac{k_{10}+k_{ic}+k_{isc}}{k_{exc}}}. \tag{2.2}$$

It is obvious that the photon emission R saturates for $k_{exc} \to \infty$

$$R_{exc\to\infty} = \frac{k_{10}}{1 + \frac{k_{isc}}{k_T}}. \tag{2.3}$$

Moreover, if one introduces the saturation intensity I_S as

$$I_S = \frac{Ik_T}{k_{exc}} \frac{k_{10} + k_{ic} + k_{isc}}{k_T + k_{isc}}, \tag{2.4}$$

the photon emission rate R can be rewritten as

$$R = R_\infty \frac{1}{\left(1 + \frac{I_S}{I}\right)}. \tag{2.5}$$

In order to determine the fluorescence quantum yield Φ_f, which relates the number of absorbed photons to the number of emitted photons, the transition $I \rightarrow 0$ or at least $I \ll I_S$ leads to

$$R_{exc\rightarrow 0} = \frac{R_\infty I}{I_S} = k_{exc}\frac{k_{10}}{k_{10}+k_{ic}+k_{isc}} = k_{exc}\Phi_f = \frac{I\sigma}{\hbar\omega}\Phi_f. \tag{2.6}$$

Φ_f consists of radiative and non-radiative components. The fluorescence lifetime τ_{Fl} is related to the rate coefficients k_{10}, k_{ic} and k_{isc} and the fluorescence quantum yield Φ_f according to

$$\tau_{Fl} = \frac{1}{k_{10}+k_{ic}+k_{isc}} = \frac{\Phi_f}{k_{10}}. \tag{2.7}$$

Based on this relations, the fluorescence lifetime is an important parameter to characterize both the intrinsic behavior of single molecules and the interactions between the molecule and its chemical and physical environment. For applications see section 2.3.

2.2 Single molecule detection in solution

The main motivation of detecting single molecules is to circumvent the averaging effect of ensemble measurements. For example, if the overall fluorescence intensity from a sample containing ten fluorescent particles is detected, the potential presence of two different species with different brightness cannot be resolved. The following section outlines the progress in the field of single molecule detection (SMD) starting from the first experiments, which raised up a lot of requirements and notes for forthcoming single molecule experiments. These considerations gave the starting signal for a very fast development in the field of SMD [104].

The first detection of a multiply labeled single molecule was reported by Hirschfeld in 1976 [42]. He used proteins labeled with 80-100 chromophores which were excited by an Argon laser operating at a wavelength of 488 nm using a total internal reflection scheme. In such a scheme, the angle of the incident laser light is sufficiently large to reflect the laser light totally at the interface between cover glass and sample volume. Only the evanescent field can enter the sample volume. Therefore, the small penetration depth of the evanescent field provided a excitation/detection volume of about 24 fl. For each labeled protein which entered the volume, the fluorescence signal was counted by a photomultiplier until a complete bleaching of the attached chromophores occurred. In another publication, Hirschfeld described the theoretical concept of time-gated fluorescence detection using pulsed lasers, which will be explained more in detail in section 2.3, and the pre-bleaching of perturbing fluorescent compounds [44]. Hirschfeld's considerations can be summarized as follows: 1) the excitation/detection volume has to be as small as possible to discriminate the fluorescence from the molecule of interest from the background luminescence; 2) SMD suffers from photo-bleaching of fluorescent molecules; 3) time-gating may provide a tool for discrimination of different fluorescent species; 4) quantum efficiencies and fluorescence lifetimes are important detection parameters [43]. Interestingly, already in 1976 Koppel and coworkers introduced a confocal detection scheme (as it will be described in section 2.3) for studying the molecular and structural mobility of fluorescent probes without going to the single molecule level [55].

It took almost 15 years until the detection of single fluorophores in solution was realized. In 1990 Shera and coworkers successfully showed the detection of single Rhodamine-6G

molecules in solution [90]. They used a mode-locked frequency-doubled Nd:YAG laser with short pulses (70 ps) and high repetition rate (82 Mhz) for exciting the molecules. The light was focused into a flow cell were the excitation of the Rhodamine-6G molecules occurred. The fluorescence was collected by a microscope objective and then spatially filtered by a slit. After passing an appropriate band pass filter, the light was detected by a microchannel-plate photomultiplier. With this set-up, it was possible to reach sufficient signal-to-noise ratios even if the applied laser intensity was so high that the Rhodamine-6G molecules were photo bleached before traveling the whole way through the detection volume. At the same time, Rigler and Widengren published the detection of single Rhodamine-6G molecules using a confocal set-up in a book chapter [81]. The main advantage of the confocal set-up was demonstrated in 1993, when Rigler and coworkers showed its superior performance in terms of the obtainable signal-to-noise ratio [80]. One year later Eigen and Rigler expanded the range of applications by showing that the binding of a labeled DNA primer to a defined or undefined DNA sequence can be monitored by using fluorescence correlation spectroscopy [18].
In 1996 Edman and coworkers showed that conformational transitions of single tetramethylrhodaminemolecules linked to a DNA sequence can be resolved using single molecule time-resolved detection [16].

2.3 Scanning confocal optical microscopy

Since the first description of a scanning confocal optical microscope (SCOM) by M. Minsky in 1955 (he filled a patent instead of publishing a scientific publication) the SCOM had become a versatile tool with well known properties in the field of fluorescence microscopy [103]. Every confocal microscope is characterized by the use of the objective both for illumination of a focal volume and for detection out of the focal volume making the basic set-up as simple as possible. A schematic diagram of a state-of-the-art SCOM as it is used for this work is shown in figure 2.2. The main principles of the set-up will be discussed in this section, whereas technical details will be discussed in section 3.2. The set-up is used with pulsed lasers instead of continuous-wave lasers to gain additional information about the fluorescent species such as the fluorescence lifetime. The repetition rates of the lasers (MHz range) are adjusted to the fluorescence lifetime in such a way that the detection of a photon can be attributed to the last laser pulse. If more than one laser is used at the same time, the synchronized laser pulses alternate and are combined into one beam using a first dichroic mirror. After adjusting the polarization by a $\lambda/2$ and a $\lambda/4$ filter, the laser light is coupled into a polarization maintaining fiber in order to obtain a point source at the end of the fiber. A lens or better an apochromatic objective with low magnification is used to obtain a parallel beam, which than reaches the second dichroic mirror. This dichroic mirror reflects the laser light to the overfilled objective (overfilled: the beam diameter of the laser is larger than the aperture of the objective), which normally has a high numerical aperture and a high magnification to realize a small, diffraction-limited volume for the excitation of the fluorophores. The objective itself is mounted to a piezo drive to change the position of the focal volume in the z-direction. To perform the scanning, the whole sample holder can be moved by additional piezo drives in the x- and/or y-direction.
Caused by the Stokes shift, the excited fluorophores emit light with a higher wavelength, which

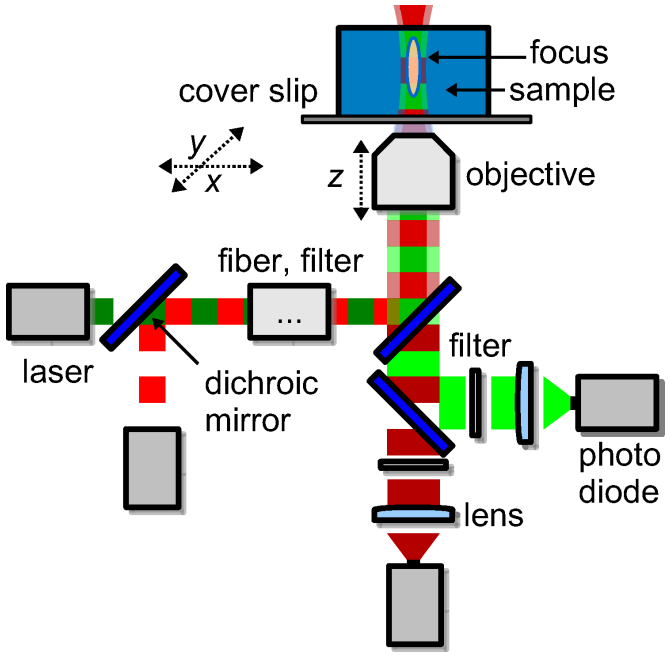

Figure 2.2: Schematic diagram of an advanced confocal microscope. Two pulsed lasers with different emission wavelengths are used for interleaved excitation of the fluorophores. The objective is used both for illumination of the focal volume and for detection out of the focal volume. The avalanche photodiode is acting as a pin-hole.

is collected by the objective and can now pass the second dichroic mirror. Further on, the wavelength range of the detected light can be either separated by a third dichroic mirror or tuned with different filter sets in order to get rid of remaining laser light or inelastic raman scattering. Afterwards, the light is focused by a lens onto the very small effective detection area of single photon counting modules (avalanche photo diodes). In this scheme, the detectors are acting as pin-holes and supress the light which is not originating from the focal plane of the microscope objective.

Time-Correlated Single Photon Counting

One of the major improvements in scanning confocal optical microscopy during the last decade was the availability of relatively cheap pulsed diode-laser sources and fast hardware for detecting the photons, whose combination allows performing time-correlated single photon counting (TCSPC). The TCSPC as it is used in this thesis works in the so-called time-tagged time-resolved (TTTR) data acquisition mode which is sketched in figure 2.3 and described in more detail in reference [102]. A pulsed laser with a sufficiently high repetition rate and a short pulse duration is used to excite a fluorescent molecule in the confocal volume. The laser and the first timer are triggered by an external source providing the possibility to measure the TCSPC-time between the arrival of a photon and the last laser pulse with a time resolution in the picosecond range. The time resolution is given by the channel width of the hardware. Additionally, the time at which a photon is detected is recorded with a resolution on the nanosecond scale on a continuous time trace to obtain the information required for Fluorescence Correlation Spectroscopy (see chapter 2.5). Even more sophisticated TCSPC-techniques provide full correlation from a picosecond to second range as described in reference [23].

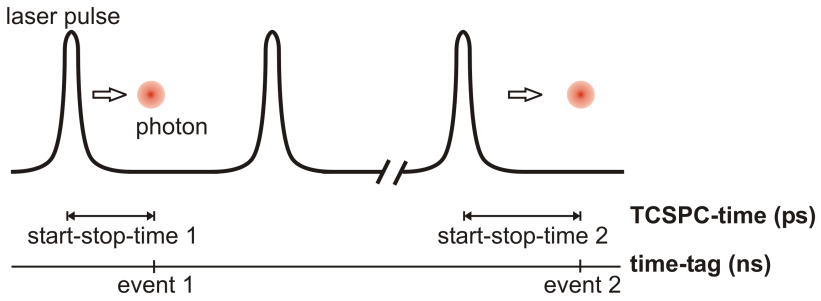

Figure 2.3: Principle of the time-tagged time-resolved (TTTR) data acquisition mode. For every photon two times are stored: a) TCSPC-time which counts the time between the last laser pulse and the detection of a photon with picosecond resolution, and b) the time-tag of every photon on a continuous time trace with nanosecond resolution.

The fluorescence lifetime (see chapter 2.1) of individual molecules can be calculated from the recorded TCSPC-times and provides thereby a versatile tool for studying different photophysical phenomena:

local environment Strickler and Berg reported in 1962 that the fluorescence lifetime of a fluorophore is proportional to $1/n^2$, where n is the environmental refractive index [94]. Thus, the fluorescence lifetime can be used to probe the environmental conditions as for example described by Suhling and coworkers [96]. They used the green fluorescent protein (GFP) as a probe in environments with different refractive indices adjusted by different concentrations of glycerol.

TRFCS The time-resolved fluorescence correlation spectroscopy (TRFCS) can be used to separate the intensity of two fluorescent species as long as the fluorescent lifetimes of the species sufficiently differ [8]. TRFCS is explained in more detail in section 2.5.

sp-FRET If a donor molecule is closer than 10 nm to an acceptor molecule, then the donor can transfer energy to the acceptor. This process decreases the fluorescence lifetime of the donor and can thereby give a quantitative value for the energy transfer. For further information see section 2.4.

rotational mobility The rotational mobility of a fluorophore can be calculated from polarization-resolved fluorescence decays [10, 92]. Thereby, one can monitor the viscosity in the vicinity of the fluorophor or binding events, which change the rotational mobility. For further information see reference [56].

For a more comprehensive review of the field see reference [95]. It is obvious that TCSPC dramatically increases the number of accessible parameters to characterize single fluorophores and there nearby chemical, physical, and biological environment.

2.4 Single pair fluorescence resonance energy transfer

One of the most frequently used techniques in the area of single molecules is the (single pair) Förster resonance energy transfer or (single pair) fluorescence resonance energy transfer

(spFRET), which allows the study of conformational changes of proteins with high accuracy and a resolution in the nanometer range [66, 89, 104, 105]. Here, emphasized by the term "single pair", we are mainly interested in the detection of only one single molecular system at the same time within the focus of the confocal microscope.

Förster published in 1948 that a distance-dependent, non-radiative energy transfer between two fluorophores can occur, as long as two preconditions are fulfilled [28]: 1) the fluorophores are in close proximity ($< 10\,\mathrm{nm}$), 2) the emission spectrum of the high energy fluorophore (*donor*) overlaps the absorption spectrum of the lower energy fluorophore (*acceptor*).

Conventionally, the used microscope consists of one laser for excitation (pulsed or continuous operating mode) of the donor and two photo diodes for a wavelength-dependent detection of the donor and the acceptor emission, respectively.

The energy transfer rate k_{fret} between the excited states $S_{1,D} \rightarrow S_{1,A}$ can be expressed using $k_{F_0,D}$ as the fluorescence rate constant of the donor in absence of the acceptor and r as the distance between the fluorophores according to

$$k_{fret} = k_{F_0,D} \left(\frac{R_0}{r} \right)^6 . \tag{2.8}$$

The distance of the fluorophores, where the probability of energy transfer by a non-radiative dipole-dipole interaction from the donor to the acceptor is 50%, is called the Förster radius R_0 reading

$$R_0 = \sqrt[6]{\frac{\kappa^2 J(\lambda)\,\Phi_D K}{n^4}}, \tag{2.9}$$

with κ as the orientation factor ($\kappa = 2/3$ for isotropic rotating systems), Φ_D as the donor quantum yield in absence of the acceptor, K as an constant ($K = 8.8 \cdot 10^{-23}\,\mathrm{mol}$), n as the refractive index of the surrounding solution and J as the overlap integral of the donor emission spectra and the acceptor absorption spectra. The overlap integral is calculated as a function of the wavelength λ

$$J = \int_0^\infty f_D(\lambda)\varepsilon_A(\lambda)\lambda^4 d\lambda, \tag{2.10}$$

with $\varepsilon_A(\lambda)$ as the molar extinction coefficient of the acceptor and f_D as the normalized emission spectrum of the donor ($\int f_D(\lambda)d\lambda = 1$).

The energy transfer efficiency E can be either determined by the change in donor lifetime $\tau_{F_1,D}$

$$E = \frac{k_{fret}}{k_{F_0,D} + k_{fret}} = \left[1 + \left(\frac{r}{R_0} \right)^6 \right]^{-1} = 1 - \frac{\tau_{F_1,D}}{\tau_{F_0,D}}, \tag{2.11}$$

where $\tau_{F_0,D}$ represents the fluorescence lifetime in absence of the donor or by comparing the measured donor and acceptor intensities I_D and I_A as

$$E = \frac{I_A}{I_A + \gamma I_D}. \tag{2.12}$$

The drawback of the second method is the incorporation of the donor and acceptor quantum yields Φ_D and Φ_A and the detection efficiencies of both channels η_D and η_A for determining

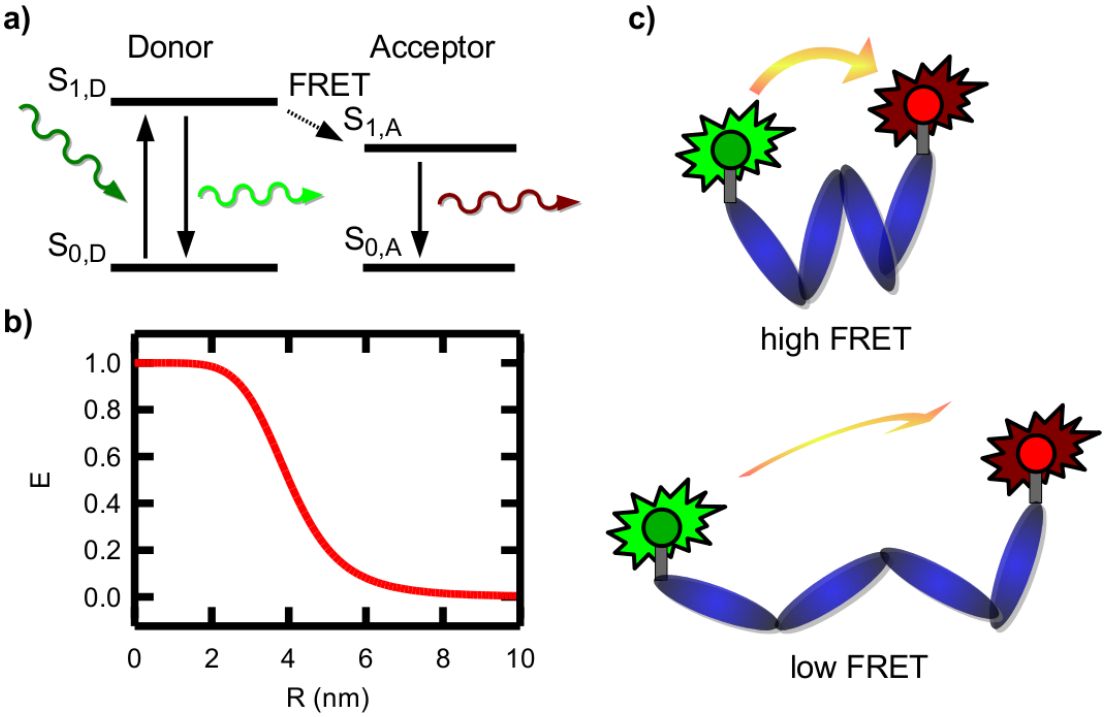

Figure 2.4: a) Simplified Jablonski diagram for FRET. After absorbing a photon, the energy in the excited state $S_{1,D}$ can be released directly by emitting a photon ($S_{1,D} \rightarrow S_{0,D}$) or indirectly after a resonant energy transfer ($S_{1,D} \rightarrow S_{1,A} \rightarrow S_{0,A}$). **b)** Energy transfer efficiency E plotted as a function of R for R_0 = 4 nm. The transfer efficiency equals 50% at R = 4 nm. **c)** Schematic diagram of a protein labeled with a donor and an acceptor. If the fluorophores are in close proximity (for example: folded protein), the probability of the energy transfer is higher than in the case of a larger donor to acceptor distance (unfolded protein).

the correction factor γ as

$$\gamma = \frac{\eta_A \Phi_A}{\eta_D \Phi_D}. \tag{2.13}$$

However, no pulsed laser set-up is necessary if only intensities are analyzed.

These considerations are summarized and visualized in figure 2.4, where **a)** shows a simplified Jablonski diagram for FRET, **b)** the distance dependency of the energy transfer using equation 2.11 with R_0 = 4 nm and **c)** a doubly labeled protein, whose potential conformational changes (folded$\rightleftharpoons$ unfolded protein) will change the observable energy transfer.

Schuler and coworkers demonstrated in 2002 that spFRET in solution can probe the energy surface of protein folding [87, 86]. In 2003 Rhoades and coworkers showed spFRET of immobilized proteins [79]. Newly developed single molecule techniques allow a time resolution on the nanosecond scale [71]. For a recent review in the field of SMS protein folding/unfolding see for example reference [66].

Alternating-Laser Excitation

However, spFRET using one laser for excitation as it has been described in the last section suffers from a number of drawbacks [51]: First, if a doubly labeled molecule (donor and acceptor) has an energy transfer efficiency close to unity (high FRET), this molecule can hardly be distinguished from a second molecule, which is only labeled with an acceptor. The first

one will show high intensities in the red detection channel and low intensities in the green one, whereas for the second molecule there is a certain probability to excite the acceptor with the green laser (this effect is known as crosstalk). Therefore, the second molecule will show a similar intensity behavior like the first one. Second, if a doubly labeled molecule has an energy transfer efficiency close to zero, there might be no sufficient difference in the intensity traces to a molecule only labeled with a donor. Third, there is no possibility to quantitatively analyze the molecular interactions. If there is an interaction in the form of $M_A + L_D \rightleftharpoons M_A L_D$, where M_A represents an acceptor-labeled macromolecule and L_D a donor-labeled ligand, the different species can not be resolved.

To overcome these drawbacks, Kapanidis, Lee and coworkers suggested in 2004 a new excitation scheme called ALEX (alternating-laser excitation) based on the use of two lasers instead of one [51]. Each of the two lasers operating in the continuous wave mode was modulated by an electro-optical modulator in association with a polarizer in such a way that an alternated excitation by either red or green laser light was achieved in order to excite the acceptor and the donor directly. The alternation period τ_{alt} was in the µs to ms range and during each excitation cycle the number of photons in both detection channels was recorded. Integrating over a certain amount of alternation cycles led to four binned intensity traces: **a)** $I_{D_{exc}}^{D_{em}}$, intensity in the donor detection channel after excitation of the donor, **b)** $I_{D_{exc}}^{A_{em}}$, intensity in the acceptor detection channel after excitation of the donor, **c)** $I_{A_{exc}}^{A_{em}}$, intensity in the acceptor detection channel after excitation of the acceptor and **d)** $I_{A_{exc}}^{D_{em}}$, intensity in the donor detection channel after excitation of the acceptor.

The calculation of the energy transfer efficiency E remains similar to equation 2.12

$$E = \frac{I_{D_{exc}}^{A_{em}}}{I_{D_{exc}}^{A_{em}} + \gamma I_{D_{exc}}^{D_{em}}}, \tag{2.14}$$

with γ as the correction factor mentioned previously. However, a new parameter S can be formulated, which represents a donor-acceptor (D- A) stoichiometry according to

$$S = \frac{I_{D_{exc}}^{A_{em}} + \gamma I_{D_{exc}}^{D_{em}}}{I_{D_{exc}}^{A_{em}} + \gamma I_{D_{exc}}^{D_{em}} + I_{A_{exc}}^{D_{em}} + I_{A_{exc}}^{A_{em}}}. \tag{2.15}$$

It can be shown that S is independent of E (supporting material in reference [51]).

If a molecule is only donor-labeled, then $S \approx 1$ because of $I_{A_{exc}}^{D_{em}} + I_{A_{exc}}^{A_{em}} \approx 0$, and if a molecule is acceptor labeled only, then $S \approx 0$ because of $I_{D_{exc}}^{A_{em}} + \gamma I_{D_{exc}}^{D_{em}} \approx 0$. Additionally, as long as $I_{A_{exc}}^{D_{em}} + I_{A_{exc}}^{A_{em}} \approx I_{D_{exc}}^{A_{em}} + \gamma I_{D_{exc}}^{D_{em}}$, the stoichiometry of doubly labeled molecules is close to $S \approx 0.5$ whereas E remains dependent on the donor-to-acceptor distance. Figure 2.5 shows a schematic diagram of an E vs. S plot separating four different species using the stoichiometry parameter S and the energy transfer efficiency parameter E.

This excitation scheme can be further improved by using pulsed interleaved lasers instead of a modulated continuous wave laser [69]. Pulsed lasers with high repetition rates in the MHz range and pulse widths of around 0.5 ns allow to relate every detected photon to the last excitation pulse as long as two requirements are fulfilled: 1) the fluorescence lifetime is shorter than the time slice between two laser pulses and 2) the mean photon count rate is much smaller than

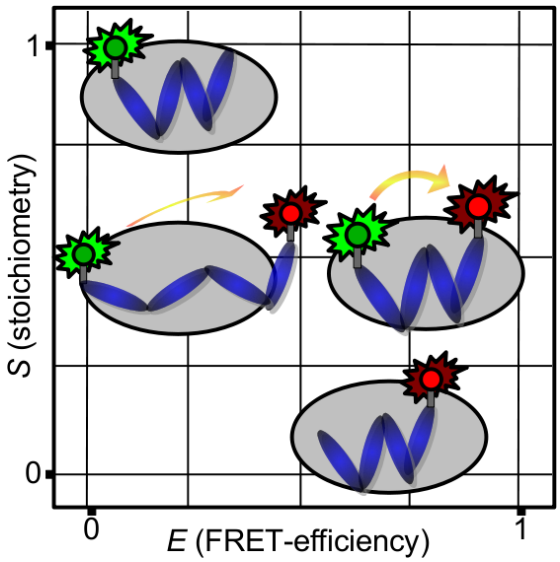

Figure 2.5: Schematic diagram of E-S plot for one donor-labeled, two doubly-labeled and one acceptor-labeled species. Without using the parameter S, a distinction of two species with almost the same (apparent) energy transfer efficiency E would not be possible.

the repetition rate of the lasers. The advantage of the last excitation scheme over that of ALEX is that one conserves the lifetime information of every detected photon.

2.5 Fluorescence correlation spectroscopy

In 1972 Magde and coworkers presented a new method to determine diffusion coefficients and particle concentrations from a detected fluctuating fluorescence signal [61]. Two landmark publications followed in 1974, which described the concept more in detail [19, 62].
Fluorescence correlation spectroscopy (FCS) is based on the fluctuation $\delta I_d(t)$ of the detectable, time-dependent fluorescence intensity $I_d(t)$ around a mean value $\langle I_d \rangle$ even under equilibrium conditions, reading

$$I_d(t) = \langle I_d \rangle + \delta I_d(t). \tag{2.16}$$

In the simplest case, the fluctuation of the fluorescence signal is caused by the Brownian motion of a few fluorescent molecules in a sufficiently small detection volume. It was shown by Rigler and coworkers, that the convolution of the collimated laser beam and the collection efficiency function can be approximated by a three-dimensional Gaussian with half axis w_0 and z_0 [80]

$$I(x,y,z) = I_0 \exp\left(-2\left(\frac{x^2+y^2}{w_0^2} + \frac{z^2}{z_0^2}\right)\right), \tag{2.17}$$

which acts as the excitation/detection focus. Let us further assume that at the time $t_0 = 0$ a single fluorescent molecule is placed in the center of the focus. Now, if the following time increment τ_1 is short enough, so that the mean free pathway of the molecule is much smaller than the size of the focus, there is a certain probability that the molecule remains within the focus at the measurement-time $t_1 = t_0 + \tau_1$. With this consideration it is obvious that the intensities detected in consecutive measurement intervals are related to each other. Generally, in FCS, the

fluctuating intensity is analyzed in terms of the intensity auto-correlation function (ACF)

$$G(\tau) = 1 + \frac{\langle \delta I_d(t) \cdot \delta I_d(t+\tau) \rangle}{\langle I_d \rangle^2}. \tag{2.18}$$

A detailed derivation of the ACF can be found in the above-mentioned references or in references [46, 112].

The ACF for the one-dimensional case of pure diffusion along the z-axis reads

$$G_{1D}(\tau) = 1 + \frac{1}{N}\left(1 + \frac{4D\tau}{z_0^2}\right)^{-\frac{1}{2}}, \tag{2.19}$$

for the two dimensional case of pure diffusion in the x-,y-plane

$$G_{2D}(\tau) = 1 + \frac{1}{N}\left(1 + \frac{4D\tau}{w_0^2}\right)^{-1}, \tag{2.20}$$

and for the three-dimensional case of pure diffusion

$$G_{3D}(\tau) = 1 + \frac{1}{N}\left(1 + \frac{4D\tau}{w_0^2}\right)^{-1}\left(1 + \frac{4D\tau}{z_0^2}\right)^{-\frac{1}{2}}, \tag{2.21}$$

where N represents the mean particle number in the detection volume and D the diffusion coefficient. Defining the diffusion time for the one-dimensional diffusion as

$$\tau_{\mathrm{D}}^{\mathrm{1D}} = \frac{z_0^2}{4D} \tag{2.22}$$

and for two- and the three-dimensional case as

$$\tau_{\mathrm{D}}^{\mathrm{2D,3D}} = \frac{\omega_0^2}{4D} \tag{2.23}$$

the ratio between the diffusion time in the one-dimensional case along z and in the three-dimensional case is just the square of the structural parameter s, which is defined as $s = z_0/w_0$ and amounts to $s \approx 4$ in a standard confocal microscope. Therefore, one can expect a 16 times longer τ_{D} inside a small channel for one-dimensional diffusion as compared to free bulk diffusion according to

$$\tau_{\mathrm{D}}^{\mathrm{1D}} = \frac{z_0^2}{4D} = \frac{s^2 w_0^2}{4D} = 16\tau_{\mathrm{D}}^{\mathrm{3D}}. \tag{2.24}$$

The ratio between the visually easier to access ACF decay half times $\tau_{1/2}$, however, is even larger due to the different exponents of the diffusion terms.

Equations 2.19 and 2.21 can be expanded in order to determine the triplet parameters of the molecules [106], reading

$$G_{1D,T}(\tau) = 1 + \frac{1}{N}\left(1 + \frac{4D\tau}{z_0^2}\right)^{-\frac{1}{2}} \frac{1 - F + e^{-\frac{\tau}{\tau_T}}}{1 - F} \tag{2.25}$$

or rather

$$G_{3D,T}(\tau) = 1 + \frac{1}{N}\left(1+\frac{4D\tau}{w_0^2}\right)^{-1}\left(1+\frac{4D\tau}{z_0^2}\right)^{-\frac{1}{2}}\frac{1-F+e^{-\frac{\tau}{\tau_T}}}{1-F}, \tag{2.26}$$

with F as the fraction of molecules in the triplet state, and τ_T as the mean duration of stay of the triplet state. Additionally, suggestions have been made to determine even rate constants as described in section 2.2 and photo-induced (back-)isomerization of dyes [106, 107], facing the problem that with a large set of fitting parameters the accuracy of each parameter determination suffers. Gennerich and Schild derived fitting functions for confined diffusion within neuronal dendrites, which feature a diameter of less than 1 µm and a length of tens of micrometers [31, 30]. For a more comprehensive review about the present use of FCS see reference [33].
In contrast to the ACF, which is calculated out of one intensity time trace, it is often useful to determine the so called cross-correlation function (CCF), which is calculated out of two intensity time traces. Therefore, the emitted beam of the fluorescent light is separated using a 50/50 beamsplitter and then focused on two detectors. The definition for the CCF

$$G_{\mathrm{CC}}(\tau) = 1 + \frac{\langle \delta I_{d,1}(t)\cdot\delta I_{d,2}(t+\tau)\rangle}{\langle I_{d,1}\rangle\langle I_{d,2}\rangle} \tag{2.27}$$

yields the same fitting functions as described previously. The advantage of using the CCF lies in the fact that one can get rid of the effect of afterpulsing. Afterpulsing is an intrinsic property of the detectors, where the detection of a real photon can be followed by a detection of a virtual photon [21, 113] and is further described in the next subsection.

Time-resolved fluorescence correlation spectroscopy

In 2002 Böhmer and coworkers introduced a new method for performing fluorescence correlation spectroscopy by using the fluorescence lifetime to separate mixtures of different fluorescent species [8]. The method is called time-resolved fluorescence correlation spectroscopy (TRFCS). In TCSPC (see section 2.3), every photon is sorted into a channel according to its arrival time after the laser pulse (TCSPC-time). Let us assume a mixture of two species; species **A** with a short fluorescence lifetime and species **B** with a sufficiently longer lifetime. It is obvious that photons which arrive shortly after the laser pulse are mainly emitted by species **A**, whereas photons which arrive almost before the next pulse are mainly emitted by species **B**. In fact, every photon can be related to one of the species with a certain probability. Generally, the intensity I_j of each channel j can be written as

$$I_j = w^{(A)}p_j^{(A)} + w^{(B)}p_j^{(B)}, \tag{2.28}$$

where $w^{(A,B)}$ represents the overall number of photons and $p^{(A,B)}$ the normalized probability of detecting photons within channel j of the respective species **A** and **B**. If a mixture of two species in terms of Fluorescence Correlation Spectroscopy needs to be separated, two filter sets $f_j^{(i)}$ (i =**A**, **B**) have to be created in such a way that they fulfill

$$\left\langle \sum_{j=1}^{L} f_j^{(i)} I_j \right\rangle = w^{(i)}, \tag{2.29}$$

where L is the total number of TCSPC channels. The brackets indicate an averaging over an infinite number of measurements. Moreover, it can be shown, assuming that photon detection follows Poissonian statistics, that with $\hat{M}_{ij} = p_j^{(i)}$ the filter sets $f_j^{(i)}$ can be calculated according to

$$f_j^{(i)} = \left(\left[\hat{M} \cdot \mathrm{diag} \left\langle I_j \right\rangle^{-1} \cdot \hat{M}^{\mathrm{T}} \right]^{-1} \cdot \hat{M} \cdot \mathrm{diag} \left\langle I_j \right\rangle^{-1} \right). \tag{2.30}$$

The $L \times L$-dimensional matrix consists of the diagonal elements $\left\langle I_j \right\rangle^{-1}$ with $j = 1, ..., L$. The approximation $\left\langle I_j \right\rangle \approx I_j$ is used for direct calculation. The patterns $p_j^{(i)}$ have to be measured independently from each other by measuring the two species in separate solutions. The filter sets $f_j^{(i)}$ and the corresponding patterns $p_j^{(i)}$ form an orthonormal system, which can be used for verification of the filter sets according to

$$\sum_{j=1}^{L} f_j^{(i)} p_j^{(k)} = \delta_{i,k}. \tag{2.31}$$

In contrast to the normal procedure of calculating the auto-correlation function, where every photon is previously weighted with a factor of 1, the weighting factor in TRFCS is $f_j^{(i)}$.
Another useful application of TRFCS is the possibility of discriminating afterpulsing from the raw data [21]. In avalanche photodiodes every absorbed photon can generate a photoelectron which then leads to further ionizations until the breakdown pulse occurs at the end. This breakdown leads to the pulse which indicates the detection of a photon. However, if some of the charge carriers remain electronically trapped for a certain time, they can be later on released by thermal excitation thereby starting a new chain of ionizations. This will cause a new pulse at the detector output now generated by a virtual photon. Due to the fact that FCS is sensitive for temporally related events, afterpulsing causes decays in the auto-correlation curve which often coincide with the decay of triplet states. In contrast to the prior use of TRFCS, where the fluorescence decay behavior of the two single species has to be known, this problem is easier to solve: Let us assume, analogous to equation 2.28, that the measured intensity per channel is a superposition of two fractions, namely the "real" data fraction **A** and the afterpulsing fraction **B**. The probability for afterpulsing follows an exponential decay with a time constant large compared to the time between two laser pulses. For this reason, the probability pattern for **B** reads $\hat{M}_{Bj} = p_j^{(B)} = L^{-1}$, where L represents the total number of TCSPC channels. For the calculation of $p_j^{(A)}$, the minimum value of I_j is substracted from every measured I_j. After the normalization it follows that $\hat{M}_{Aj} = p_j^{(A)} = \sum I_j / \left(I_j - \mathrm{Min}(I_j) \right)$. The calculation of the filter sets is straightforward using equation 2.30 and taking $\left\langle I_j \right\rangle \approx I_j$.

Influence of uncorrelated background

If the diffusion of single molecules is confined to host materials, this may cause additional uncorrelated background luminescence. Either caused by the material itself or by adsorption of probe molecules onto the host material, the background influences the behavior of the auto-correlation function. Even if the mean diffusion time τ_D remains unchanged, the amplitude of the auto-correlation function is getting smaller with increasing background luminescence. As mentioned above, the amplitude is inversely proportional to the number of apparent molecules

within the focus. Based on the work of Koppel in 1974 [54], the following equation was derived by Milon and coworkers [67] in order to relate the calculated apparent number of molecules N to the real number of molecules N' and the (apparent) number of molecules N_{noise} given by the (uncorrelated) background according to

$$N = \frac{(N' + N_{noise})^2}{N'} \tag{2.32}$$

with

$$N_{noise} = \frac{\text{background count rate per second}}{\text{count rate per molecule per second}} = \frac{\langle I_{Bg} \rangle}{\langle I \rangle - \langle I_{Bg} \rangle} N', \tag{2.33}$$

where $\langle I_{Bg} \rangle$ is the (estimated) mean background intensity and $\langle I \rangle$ the measured mean intensity. If the presence of (uncorrelated) background cannot be completely neglected, the real number of molecules N' in the focus is always smaller than the calculated one without background correction.

2.6 Orientation determination: from 2-D to 3-D

Beside using single molecules for spFRET as described in section 2.4, another unique feature of single molecules is their absorption and emission anisotropy due to the well-defined transition dipole(s) for both processes allowing the determination of the molecule's orientation. As shown in figure 2.6 **a)**, the orientation of a vector in spherical coordinates is fully determined by the polar angle θ and the azimuthal angle ϕ. Whereas the determination of θ is quite sophisticated, the determination of ϕ is more straightforward. Figure 2.6 **b)** shows that by using a polarizing beamsplitter in front of two detectors the detectable light can be divided into its horizontal and vertical components. However, it has to be emphasized that the simple relation $\tan\phi = I_{c,0}/I_{c,90}$ does not hold for using microscope objectives with high numerical aperture. Historically, the first polarization-resolved techniques performed at single molecules were based on a different concept (for orientation determination in steady-state fluorescence polarization microscopy see reference [1]). Instead of detecting polarization-resolved intensities, the polarization of the laser light was modulated before exciting the single molecules. Note that ϕ corresponds to the azimuthal angle of the emission transition dipole, which does not coincide with the azimuthal angle α of the absorption transition dipole in any case [36]. In 1993 Güttler and coworkers published a method, where the polarization of the laser light was changed with a $\lambda/2$ retardation plate [34]. The polarized light was used to excite single pentacene molecules in a p-terphenyl matrix. The measured intensity is a function of the azimuthal angle ϕ and was used to show the existence of two structural domains. In 1994 Xie and coworkers used two polarization directions (0° and 90°) to show that dipole rotation is the origin of emission jumps in sulforhodamine 101 adsorbed on glass [110]. A very accurate determination of the in-plane dipole angle α was demonstrated by Ha and coworkers in 1996 [35]. Single molecules were excited in the far field with linearly polarized light. The polarization angle ψ was continuously modulated in the millisecond range using an electro-optical modulator. Thus, the detected emission signal can be plotted as a function of ψ. Assuming that the emission signal I_{em} is a function of the absorption transition dipole $\vec{\mu}$ and the electrical

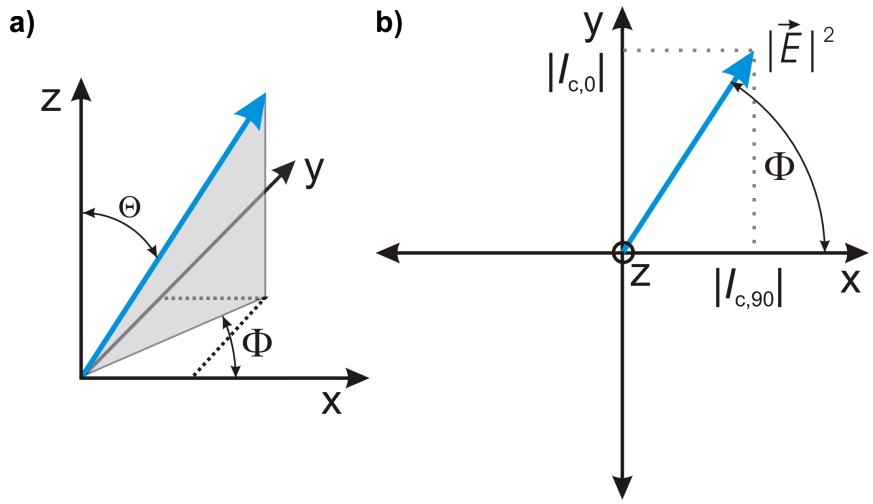

Figure 2.6: **a)** The orientation of a vector in spherical coordinates is fully determined by the polar angle θ and the azimuthal angle ϕ. **b)** Polarization-resolved techniques are using a projection of the transition dipole to determine the azimuthal angle ϕ. Here, a polarizing beamsplitter is used to divide the detectable light into its horizontal ($I_{c,0}$) and vertical ($I_{c,90}$) components.

field vector $\overrightarrow{E}$ according to

$$I_{em} \propto \left| \overrightarrow{\mu} \cdot \overrightarrow{E} \right|^2, \tag{2.34}$$

the detected modulated intensity can be fitted using

$$I_{em} = I_0 \cos^2(\psi - \phi) + I_{back}, \tag{2.35}$$

where I_0 is the signal intensity and I_{back} the background intensity. Moreover, this technique can resolve desorption and re-adsorption of single molecules from and onto the coverslip but suffers from the high number of photons which have to be detected in order to achieve sufficient accuracy. A more detailed description of the method can be found in reference [36]. In 1997 Sase and coworkers resolved the axial rotation of sliding actin filaments by exciting the fluorophores with circularly light and separating the emitted fluorescence with a polarizing beamsplitter [83].

Three-dimensional orientation determination

As mentioned above, the determination of the full three-dimensional orientation of single molecules is much more sophisticated. In the following, several methods will be discussed, which have been proposed in the literature.

Betzig and Chichester showed in 1993 that a near-field scanning optical microscope can be used to determine the accurate position and the three dimensional orientation of single fluorophores [5]. Unexpectedly, the imaged molecules did not appear as identical peaks with comparable width but rather as a distribution of ellipsoidal and symmetric peaks or rings and arcs. These patterns can be calculated for various orientations taking into account the interaction of the electric dipole of the molecule with the incident electromagnetic field from the aperture. In 1999 Bartko and coworkers published a detection sheme using a confocal microscope operating in a total internal reflection mode between the sample/air interface with CCD wide-field

detection [2]. After slightly defocussing the molecules in the z-direction, the imaged intensity patterns were used to determine the orientation of the molecules by applying an appropriate fitting-model. A similar pattern approach is described in reference [7]. Instead of using slight defocussing, different directions of incidence with linearly polarized light can be used for orientation determination, resulting in a shot noise-limited angular resolution of 2° [78]. For the case of using highly symmetric single chromophores (e.g. CdSe quantum dots) Empedocles and coworkers demonstrated in 1999 that comparing the fluorescence intensity as a function of the polarization angle is sufficient for a three-dimensional orientation determination [20].
Several other publications deal with more complex excitation schemes. Sick and coworkers used an annular illumination geometry approach, where the inner part of the laser beam is cut off [91]. Again, the imaged intensity patterns can be attributed to different orientations without loosing the spatial information as it occurs with the defocussing techniques. Hübner and coworkers used this scheme to determine the donor and acceptor transition dipoles in individual molecules, which is crucial to reliable distance determination based on FRET [50]. Forkey and coworkers used four different excitation polarizations in a total internal reflection scheme to measure the structural dynamics of the light chain domain of brain myosin V with a time resolution of up to 20 ms and without the need of any fitting procedure [25]. Nearly at the same time Vacha and Kontani presented a set-up combining a TIRF-illumination scheme with epi-fluorescence detection [101]. They also achieved an orientation determination without additional fitting procedures. In 2004 Debarre and coworkers reported that so called out-of-plane molecules, where the absorbing dipole coincides with the z-axis, can be detected more easily if amplitude and phase masking is applied to the input beam [12]. In a theoretical work, Fourkas predicted that comparing the fluorescent light intensities of three polarization directions would be sufficient to determine ϕ and θ [26].
Even though a number of methods was proposed for a full three-dimensional orientation determination of the absorption/emission dipole of single molecules, yet no fast easy-to-use approach is available. This problem will be addressed in chapter 5.

2.7 Geometrical confinement of diffusion

Single molecule detection of freely diffusing molecules suffers from two limitations. First, the transit time of the freely diffusing molecules through the confocal volume restricts the timescale of internal dynamics that can be explored. It is obvious that the longer a single molecules stays within the confocal focus the more photons can be detected from that specific molecule. Second, in a typical single molecule experiment in solution, the concentration of sample molecules is limited to less than one nanomol per liter to keep the probability of double occupancy low. However, systems that involve ligand binding or chemical change do often require micromolar or higher reagent concentrations [58]. Unfortunately, both limitations mostly interact with each other: Reducing the effective excitation/detection volume will lead to shortened transit times of the diffusing molecules.
The excitation/detection volume can be reduced in two different ways. One way is to reduce the excitation volume, where different methods have been proposed:
STED: The stimulated emission depletion was theoretically described by Hell and Wichmann

in 1994 [41] and gained a lot of attention after its experimental realization [40, 53]. This technique consists of a conventional confocal excitation spot which is overlapped with a STED spot featuring a central naught. The STED spot is created by a pulsed laser with higher wavelength than the excitation wavelength and a $\lambda/2$ wave plate in the center of the beam and efficiently depletes the first excited state of a fluorophore at high intensities in its accessible volume. Therefore, the effective excitation spot is drastically minimized to 0.67 attoliter (10^{-18} l) and an optical resolution of around 30 nm can be obtained, which is far beyond the diffraction limit.
TIRF: In a total-internal-reflection-fluorescence scheme a large angle of the incident laser light excludes light propagation trough the glass/water interface. However, evanescent fields can enter the sample volume [42, 93]. The excitation volume is reduced by the fact that the penetration depth of the evanescent field in an aqueous solution is less than 200 nm.
SNOM: Similar to TIRF the direct light propagation in a scanning near-field optical microscope is prevented and only evanescent fields can enter the volume of interest [5]. In SNOM a tapered fiber tip with a diameter of less than 100 nm is covered with a metal at the side to fulfill this requirement.
Zero-mode waveguides: Zero-mode waveguides consist of sub-wavelength holes in a thin metal film deposited on a glass substrate. Again, the propagation of light through the metal film is forbidden and only evanescent fields occur within the holes [59]. With this method observation volumes of zeptoliters (10^{-21} l) can be achieved. Moreover, Samiee and coworkers derived an empirical FCS model accounting for one-dimensional diffusion within the tubes and used this technique to measure oligomerization of the bacteriophage λ repressor protein at micromolar concentrations [82].
Besides reducing the excitation volume with the methods described above, restricting the accessible space of the detectable diffusing fluorophores is another possible strategy for efficient single-molecule detection. An example from a biological system are dendrites of cultured neurons [31, 30]. These dendrites are cellular extensions of the neurons, where the majority of input to the neuron occurs. They feature a thickness (diameter) of less than 1 µm and a length of several tens of micrometers. Other examples of reducing the effective detection volume are presented in the following: **1)** Cone-shaped micro-capillaries with an inner diameter of less than 1 µm were used to confine the diffusion of single molecules [111]. The flow of the conjugates was established using electrokinetic forces. Due to the fact that the path of motion of the molecules is confined and thereby known, the obtainable signal-to-noise ratio is increased compared with measurements in free solution [15]. Sauer and coworker proposed the use of micro-capillaries for DNA sequencing [84]. **2)** Mesostructured molecular sieves were used to observe the translational diffusion of single terrylenediimide molecules [88]. **3)** In recent years, nanofluidic devices for single molecule detection fabricated by lithographic methods have gained more and more attention [64]. This is mainly attributed to the availability of advanced lithographic techniques such as electron beam lithography, reactive ion etching et cetera. Han and coworkers reported on the separation of long DNA molecules using entropic trap arrays [38] and Foquet and coworkers showed the focal volume confinement by single fluidic channels featuring a channel width down to 350 nm [24].
Even tough a reduction of the effective detection volume can be achieved with several methods, it remains a challenge to combine reduced detection volumes with increased observation time.